

**Supporting Information**

**Gas-Liquid Flow and Mass Transfer in an Advanced Flow  
Reactor**

María José Nieves-Remacha<sup>1</sup>, Amol A. Kulkarni<sup>1,2</sup>, and Klavs F. Jensen\*,<sup>1</sup>

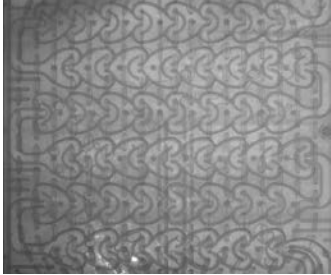
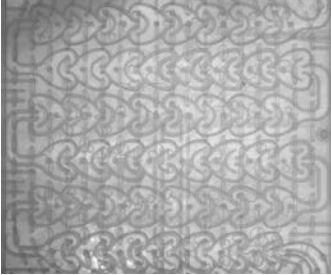
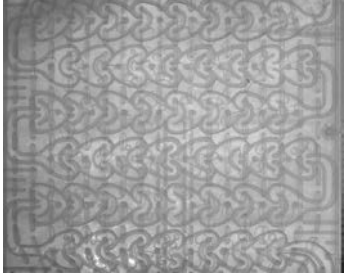
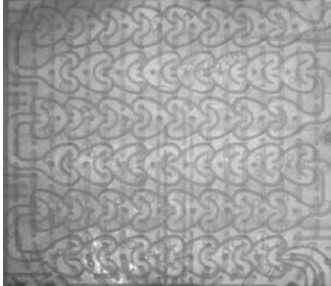


<sup>1</sup>Dept. Chem. Eng., Massachusetts Institute of Technology, Cambridge, MA 02139, USA

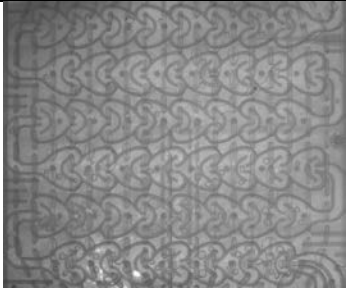
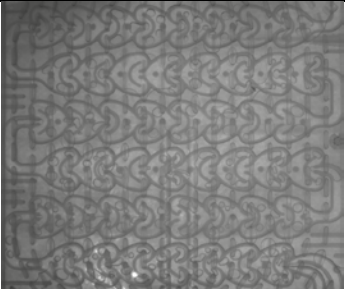
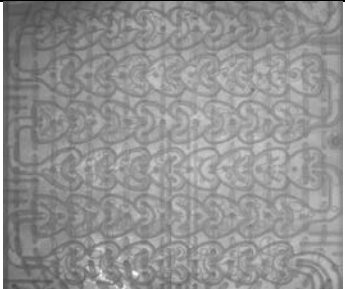
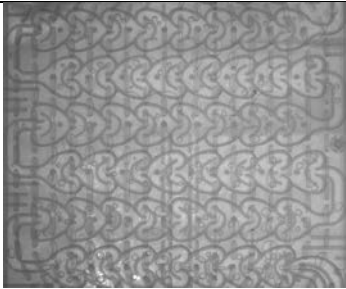
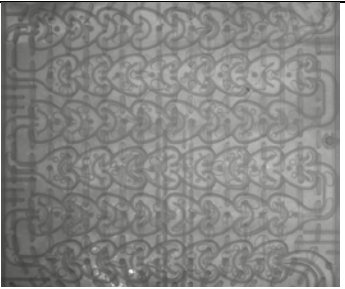
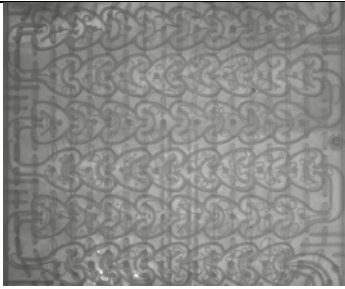
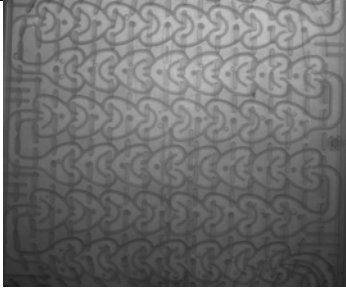
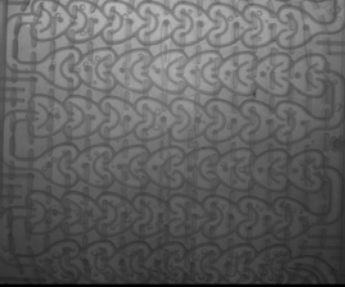




<sup>2</sup>CEPD, CSIR-National Chemical Laboratory, Pune 411008, India

1. Images of the gas-liquid flow in the AFR module in horizontal orientation

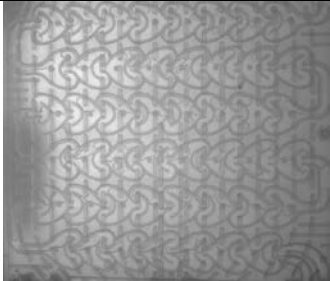
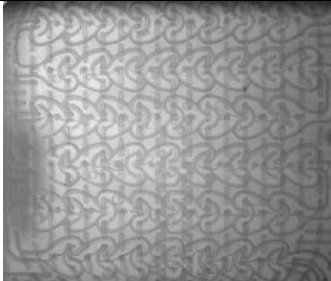

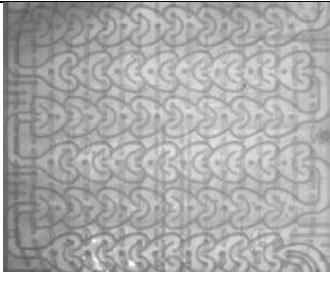
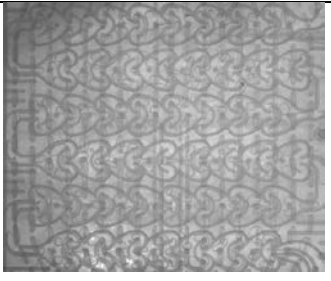
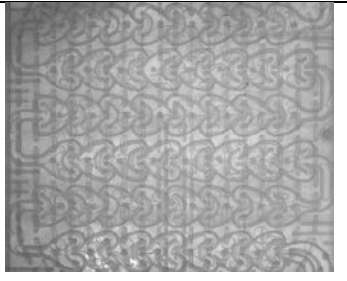
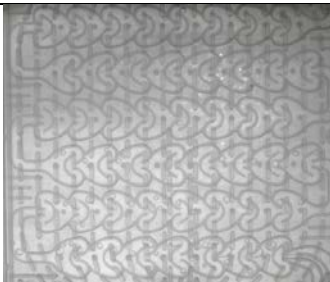
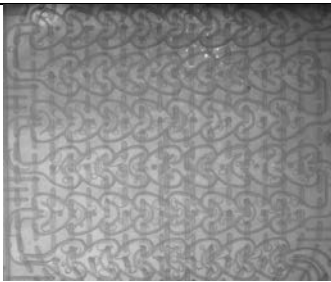
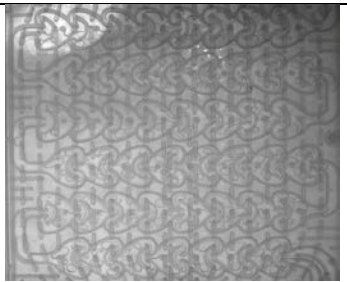
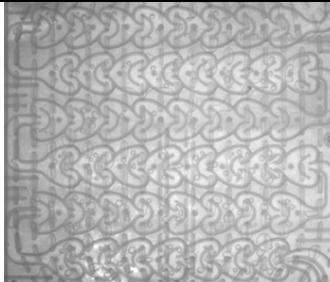
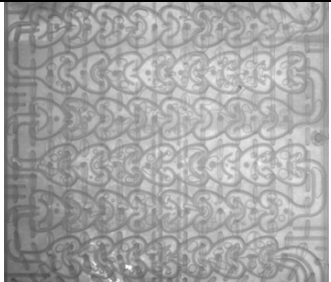
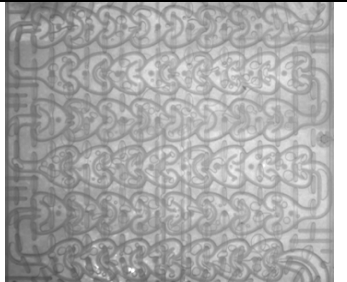
1. Images of the gas-liquid flow in the AFR module

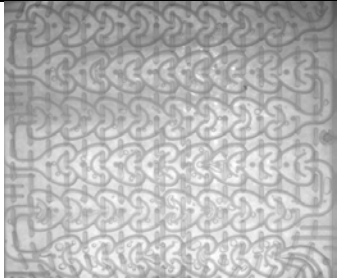
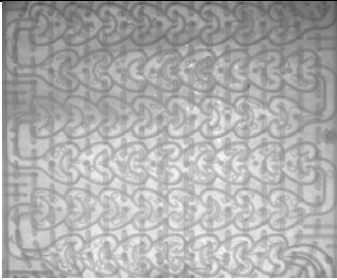
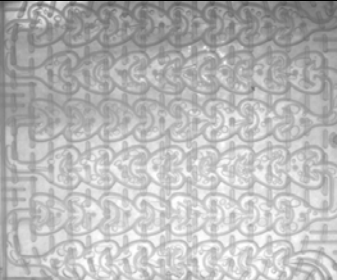
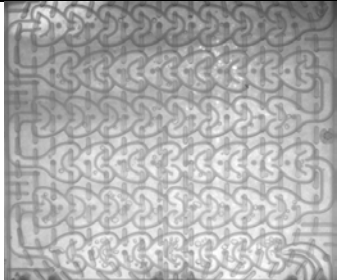
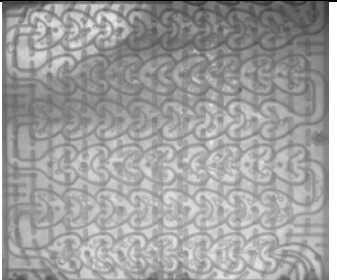
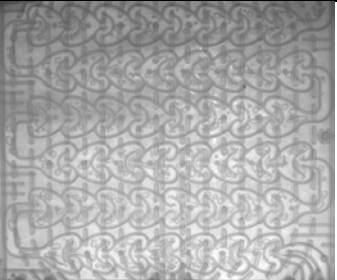
A) Horizontal orientation

Q <sub>L</sub> \	Gas flow rates (Q <sub>G</sub> )		
10 ml/min	 5.6 ml/min	 20.8 ml/min	 35.8 ml/min
20 ml/min	 13.3 ml/min	 35.8 ml/min	 73.3 ml/min

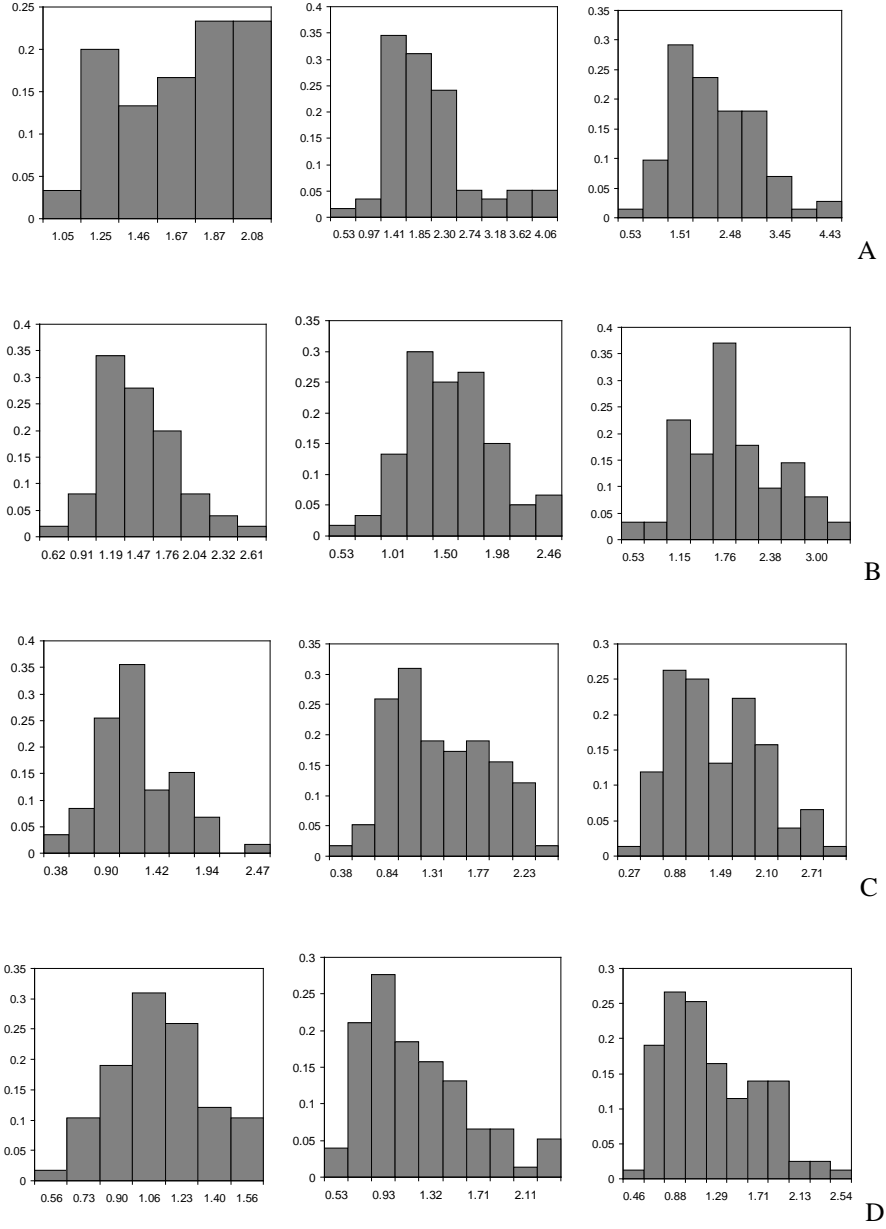
30 ml/min			
	13.3 ml/min	35.8 ml/min	73.3 ml/min
40 ml/min			
	26.8 ml/min	58.3 ml/min	70.3 ml/min
60 ml/min			
	23.8 ml/min	35.8 ml/min	77.8 ml/min
80 ml/min			
	35.8 ml/min	73.3 ml/min	88.2 ml/min

B) Vertical orientation

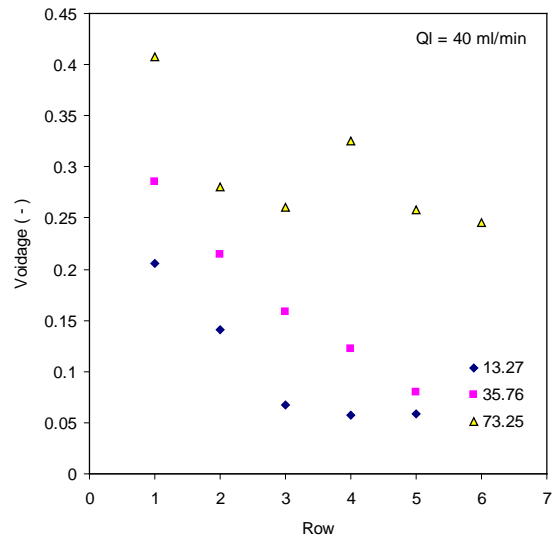
$Q_L$	Gas flow rates ( $Q_G$ )		
10 ml/min	 13.3 ml/min	 35.8 ml/min	 70.3 ml/min
20 ml/min	 5.8 ml/min	 35.8 ml/min	 73.3 ml/min
30 ml/min	 13.3 ml/min	 35.8 ml/min	 65.8 ml/min
40 ml/min	 26.8 ml/min	 58.3 ml/min	 70.3 ml/min

60 ml/min			
	24 ml/min	73 ml/min	106 ml/min
80 ml/min			
	24 ml/min	73 ml/min	106 ml/min

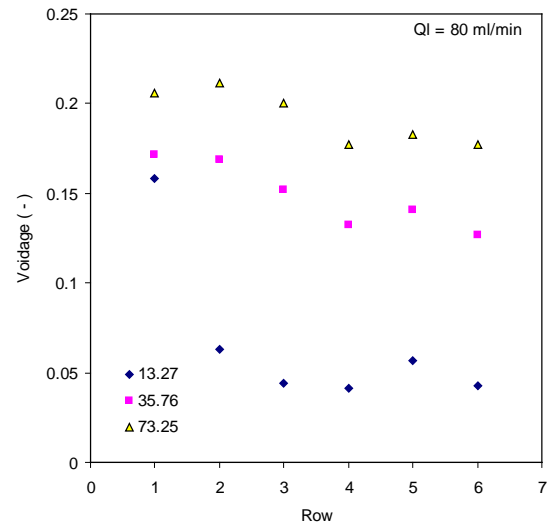
**Figure SI-1:** Images of AFR taken for G-L flow at different gas and liquid flow rates.



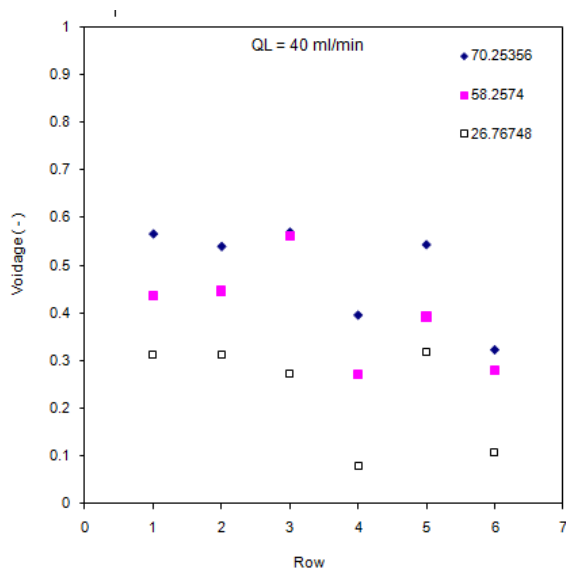
**Figure SI-2:** Bubble size distribution in the AFR at different gas and liquid flow rates for vertical orientation. Gas flow rates are given from left to right for every liquid flow rate. (A)  $Q_L = 20$  (ml/min),  $Q_G = 13, 36, 66$  ml/min, (B)  $Q_L = 30$  (ml/min),  $Q_G = 21, 36, 66$  ml/min, (C)  $Q_L = 60$  (ml/min),  $Q_G = 36, 73, 103$  ml/min, (D)  $Q_L = 80$  (ml/min),  $Q_G = 36, 79, 103$  ml/min.



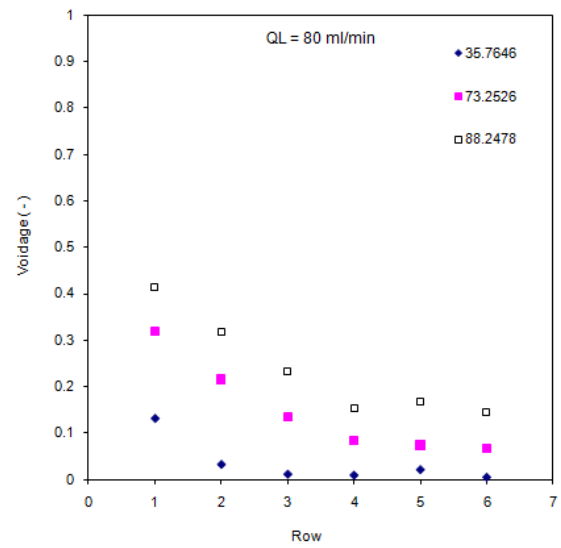
A



B

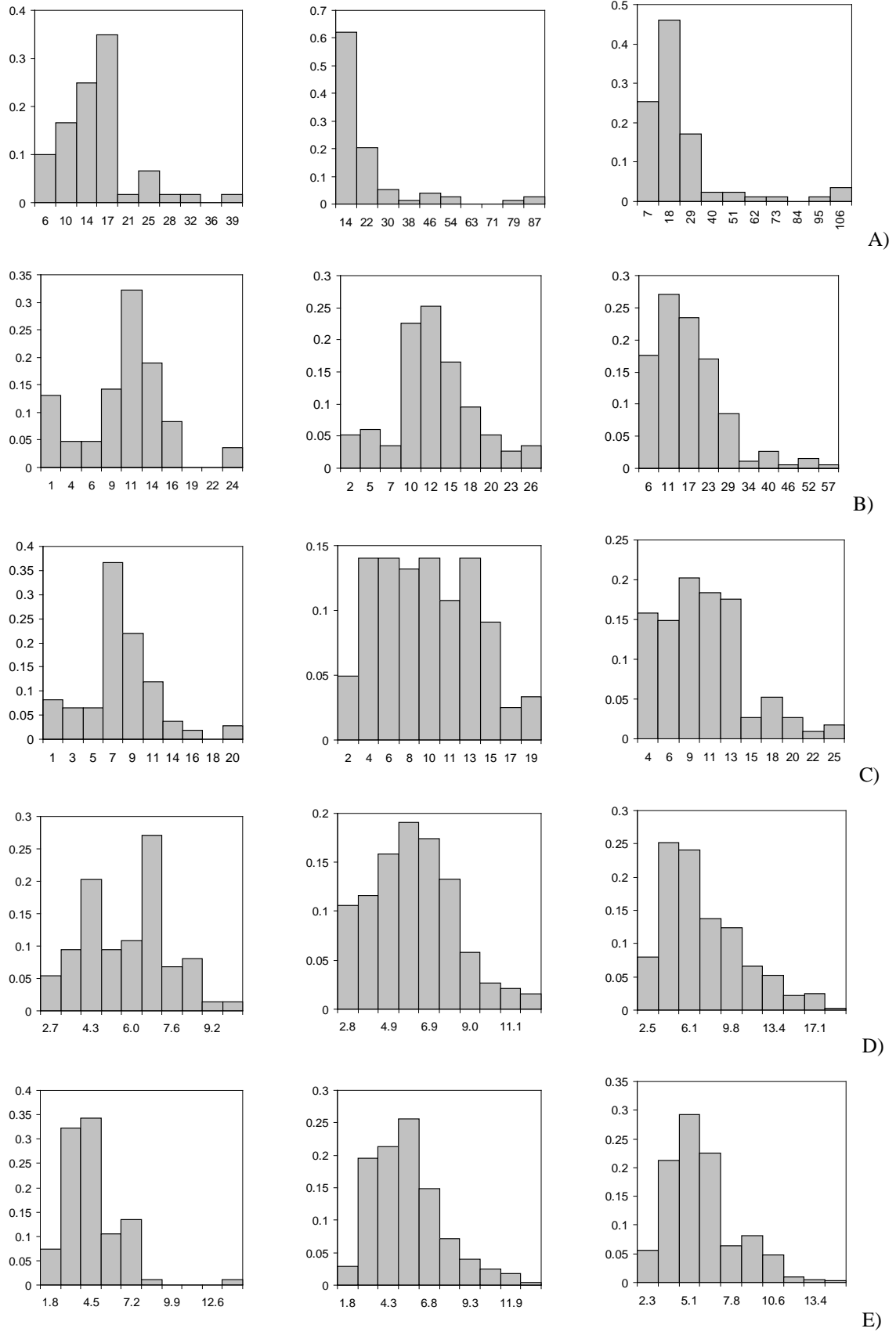


C

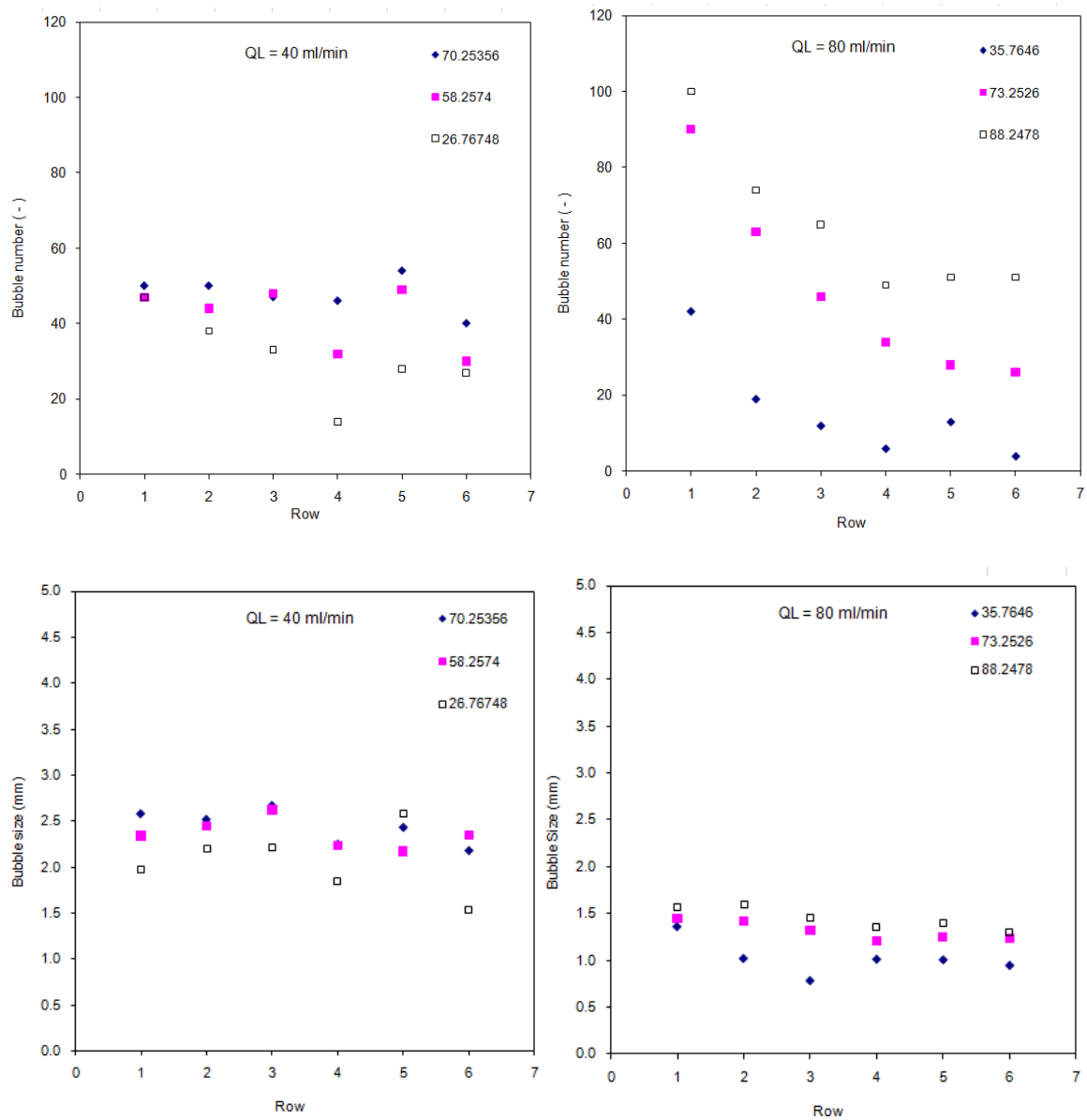


D

**Figure SI-3:** Change in the fractional gas holdup along the length of the AFR for (A-B) Vertical orientation of module, (C-D) horizontal orientation of module.



**Figure SI-4:** Bubble size distribution in the horizontal orientation of the AFR. (a)  $Q_L = 10 \text{ ml/min}$ ,  $Q_G = 6, 13, 36 \text{ ml/min}$ , (b)  $Q_L = 20 \text{ ml/min}$ ,  $Q_G = 13, 36, 73 \text{ ml/min}$ , (c)  $Q_L = 40 \text{ ml/min}$ ,  $Q_G = 27, 58, 70 \text{ ml/min}$ , (d)  $Q_L = 60 \text{ ml/min}$ ,  $Q_G = 24, 36, 78 \text{ ml/min}$ , (e)  $Q_L = 80 \text{ ml/min}$ ,  $Q_G = 36, 73, 88 \text{ ml/min}$ .



**Figure SI-5:** Variation in the bubble number and bubble size along the length of the AFR in horizontal orientation



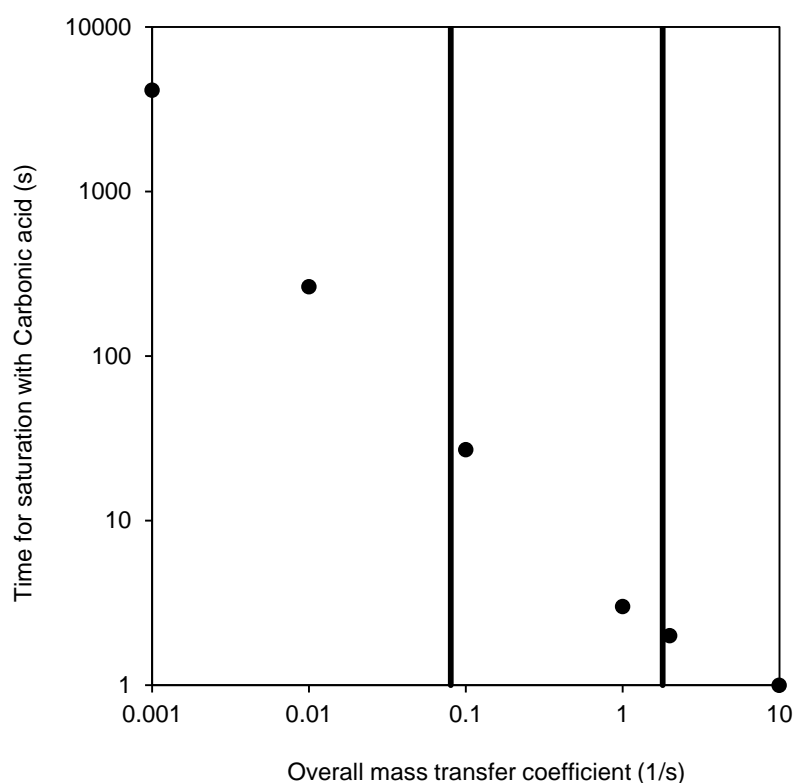
### Effect of change in pH along the reactor length on $k_L$ in AFR

It is known that the absorption of CO<sub>2</sub> in water gets retained as carbon dioxide, carbonic acid, bicarbonate ion, and carbonate ion. The equilibrium concentrations of these individual species depend upon local pH. In all the experiments, Millipore water was used. Since both the phases are continuous, the dissolution of CO<sub>2</sub> resulted in a change of pH along the length of the flow path. However, the extent of dissolution depends upon the local pH values and hence the rate of mass transfer would change along the length of the reactor. Following the approach by Hill<sup>27</sup> the concentration of carbonic acid in water was predicted (using the below differential equation) for the case of a flow reactor over a wider range of overall mass transfer coefficient values.

$$\frac{d[\text{H}_2\text{CO}_3]}{dt} = K_L a([\text{H}_2\text{CO}_3]^* - [\text{H}_2\text{CO}_3]) \times \left(1 - \frac{K_1}{K_1 + (K_1[\text{H}_2\text{CO}_3])^{0.5}}\right)$$

The values and details on different parameters in the above equation can be seen in Hill.<sup>27</sup> Assuming that individual heart zones are very well mixed, every heart zone will show a different mass transfer rate due to reduced concentration difference between the bulk liquid and the gas phase in addition to the changed pH of the solution where the dissolved CO<sub>2</sub> is in decomposed state. Since the AFR is a continuous flow system with very low back-mixing from one heart cell to the other, the effect of change in pH is a steady state phenomenon along the length of the reactor without any back-mixing. The observations indicate that for a given inlet concentration, the values of slip velocity and the bubble size (i.e. the overall mass transfer coefficient) decide the time required for reaching the maximum concentration of carbonic acid during which the rate of mass transfer gradually decreases. Thus, the AFR would show behaviour similar to a sequence of completely mixed reactors along the length of reactor and the rate of absorption of CO<sub>2</sub> would reduce along the length of reactor. However (i) reduction in bubble size along the flow path would lead to increase in the specific

interfacial area, and (ii) smaller gas phase holdup and smaller bubble size would yield lower slip velocity thereby yielding relatively smaller individual mass transfer coefficient. The simulated values of saturation time for the range of  $k_L a$  for AFR are shown in Figure SI-pH Effect. The data indicates that a residence time of maximum of 20 s per AFR module (i.e.  $Q > 24$  ml/min) is suitable to overcome the typical mass transfer limitations in a gas-liquid reactor. However the actual values would vary depending upon the physicochemical properties of the reacting fluids.



**Figure SI-6** (pH Effect): Simulated time required for the saturation of water with carbonic acid resulting from absorption of  $\text{CO}_2$ . The vertical lines indicate the range of  $k_L a$  estimated for AFR based on the slip velocity calculations.

## Materials and Methods: Reproducibility of Measurements

In order to study the reproducibility of the measurements, two cases were considered: a) three measurements of the size of a single bubble were performed by measuring the perimeter using the software ImageJ and calculating the diameter from the perimeter. The mean value ( $\bar{X}$ ) and standard deviation (s) were then calculated; b) three measurements of all the bubbles encountered within one single heart cell for a single experiment were performed, and the mean value and standard deviation of the three measurements of the number average bubble size were calculated. A confidence interval (CI) of 99.5% probability for a  $t_{student}$  of 9.925 was then calculated.

**Table 1: Reproducibility of Measurements. Case a) Single Bubble.**

Measurement	Bubble Size (mm)	Average (mm)	Standard Deviation (mm)	Confidence Interval (99.5%)
1	1.300	1.333	0.047	0.27
2	1.400			
3	1.300			

**Table 2: Reproducibility of Measurements. Case b) Single Heart Cell.**

Measurement	Average in Heart Bubble Size (mm)	Average Bubble Size (mm)	Standard Deviation (mm)	Confidence Interval (99.5%)
1	1.258	1.325	0.067	0.38
2	1.300			
3	1.427			

The uncertainty in the experimental measurement of bubble size is propagated in the estimation of derived variables that depend functionally on the bubble size. This has been taken into account in the estimation of gas holdup, specific interfacial area, and mass transfer coefficients.